

A panorama of excited-state g -factor measurements: advancing moment measurements on radioactive beams

Andrew E. Stuchbery

Department of Nuclear Physics, Research School of Physics and Engineering, The Australian National University, Canberra, ACT 0200, Australia

E-mail: andrew.stuchbery@anu.edu.au

Abstract. Patterns in the systematics of g factors for the first excited states of even-even nuclei are explored across the nuclear landscape for heavy nuclei ($A > 90$). The pathway to collectivity from semimagic to mid-shell nuclei is discussed, and attention given to the different behavior of nuclei either side of $N = 82$. As most $g(2_1^+)$ data is for nuclides near the valley of stability, the development of the recoil in vacuum technique for moment measurements on radioactive beams is discussed, with particular attention given to the free-ion hyperfine fields of Se and Ge ions leaving carbon foils with velocities of about 5% of the speed of light.

1. Introduction

In the first part of this paper, the gyromagnetic ratio systematics for the first-excited states in even-even nuclei, $g(2_1^+)$, are examined across the nuclear chart. The focus is on overall trends as well as the path from spherical to deformed nuclei and the role of g factors as a microscopic probe of the onset of collectivity. The evolution of nuclear structure is often discussed in terms of the ratio $R_{42} = E(4_1^+)/E(2_1^+)$ (see for example [1] and references therein). Figure 1 shows a nuclear chart with R_{42} values indicated by color, along the lines of Cakirli and Casten [2], but restricted to nuclides with $10 \leq Z \leq 82$ for which $g(2_1^+)$ is known. It is apparent that the $g(2_1^+)$ data are much less extensive than R_{42} data, and mainly cluster around the valley of stability. The second part of this paper therefore concerns the developing opportunities to perform g -factor measurements in new regions of the nuclear chart. The focus is on g -factor measurements on radioactive beams by the recoil-in-vacuum (RIV) technique [3, 4].

2. A panorama of excited state g factors in heavy nuclei: experimental trends

The trends in $g(2_1^+)$ values for medium to heavy nuclei have been discussed previously. It is timely, however, to reconsider these systematics in the light of theoretical advances (see below) and the availability of new data, which either increase the span of the data set (e.g. [5]) or significantly improve the precision (e.g. [6]). Discussion here will be on the three regions labeled in figure 1. It is convenient to begin with the heaviest region bounded by the $50 \leq Z \leq 82$ and $82 \leq N \leq 126$ shells, which will be referred to as the ‘rare earth region’. The second region, the ‘ $A \sim 130$ ’ region, includes nuclei near ^{132}Sn having $Z > 50$ and $N \leq 82$. Finally, the ‘ $A \sim 100$ ’ region has nuclei with $40 \leq Z < 50$ and $50 \leq N < 80$.

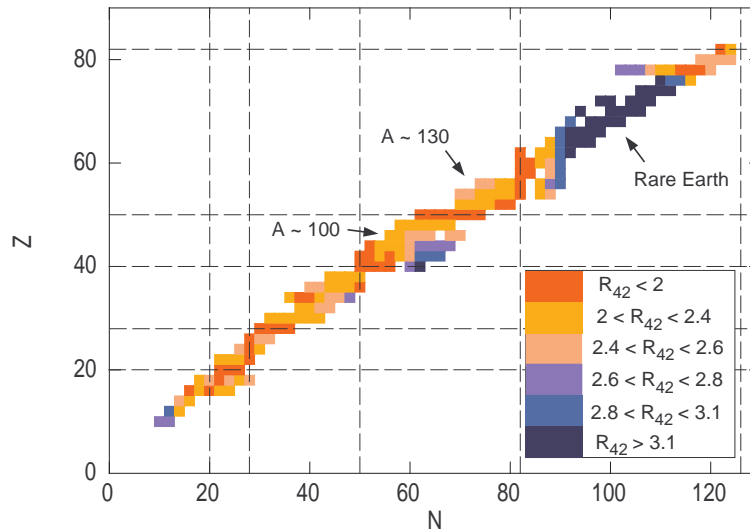


Figure 1. Chart of the nuclides showing nuclei between $Z = 10$ and $Z = 82$ for which $g(2_1^+)$ has been measured. The color indicates $R_{42} = E(4_1^+)/E(2_1^+)$ for each nuclide. Dashed lines indicate magic numbers.

To expose and investigate trends in nuclear moments for heavy nuclei, plots were made of $g(2_1^+)$ versus alternative variables such as R_{42} , N , and the valence proton fraction, N_p/N_t , where N_p is the number of valence protons or proton holes relative to the nearest magic number, and N_t is the total number of valence nucleons (protons plus neutrons) counted in the same way. Patterns and contrasting behavior proved most apparent when $g(2_1^+)$ was plotted versus N in the $A \sim 100$ region (see figure 2), and versus N_p/N_t in the $A \sim 130$ and rare-earth regions (see figures 3 and 4, respectively). Color has been used to indicate the R_{42} value associated with each measured g factor.

Looking first at the rare-earth region ($50 \leq Z < 82$ and $82 \leq N < 126$) and figure 2, it can be seen that the data for $N_p/N_t < 0.7$ cluster around a straight line, which can be interpreted in terms of the proton-neutron Interaction Boson Model expression $g = g_\nu + (g_\pi - g_\nu)(N_p/N_t)$. Although the boson g factors from the fit, $g_\nu = 0.23$ (neutrons) and $g_\pi = 0.45$ (protons), depart significantly from the nominal boson g factors, $g_\nu = 0$ and $g_\pi = 1$, the trend for an increase in $g(2_1^+)$ as the shell closures at $N = 82$ and $N = 126$ are approached is correct; in contrast, this experimental feature of the rare-earth region is contrary to the Z/A estimate, even when corrections for pairing are included [7].

It is known from observables such as R_{42} that heavy nuclei make a rapid transition from spherical to deformed behavior. The rapidity of this transition is evident in the g factors of the rare-earth nuclei as well. Aside from the semimagic $N = 82$ isotones, the nuclei that show strong departures from the collective trend line all have $R_{42} < 2.4$, and 4 or fewer valence neutrons. For the $N = 82$ nuclei $g(2_1^+) \sim 1$, the specific value being determined by the particular proton configuration. Then, with the addition of two neutrons, $g(2_1^+)$ falls well below the collective trend.

As shown in figure 3, in the $A \sim 130$ region the data for isotopes with $N_p/N_t < 0.7$ again cluster around a straight line, here characterized by $g_\nu = 0.31$ and $g_\pi = 0.38$. In contrast with the rare-earth region, there are no cases near $N_p/N_t = 0.8$ where the g factors undershoot the collective trend. The reason for this difference will be discussed below.

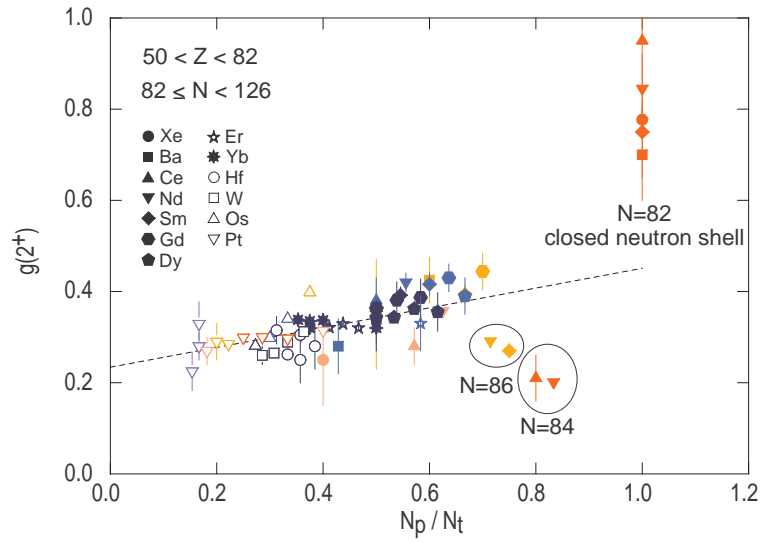


Figure 2. $g(2_1^+)$ as a function of the valence proton fraction for nuclei with $50 \leq Z < 82$ and $82 \leq N < 126$. The broken line indicates the trend for $N_p/N_t < 0.7$. Data points (from [8]) are colored to indicate R_{42} . See figure 1 for color key.

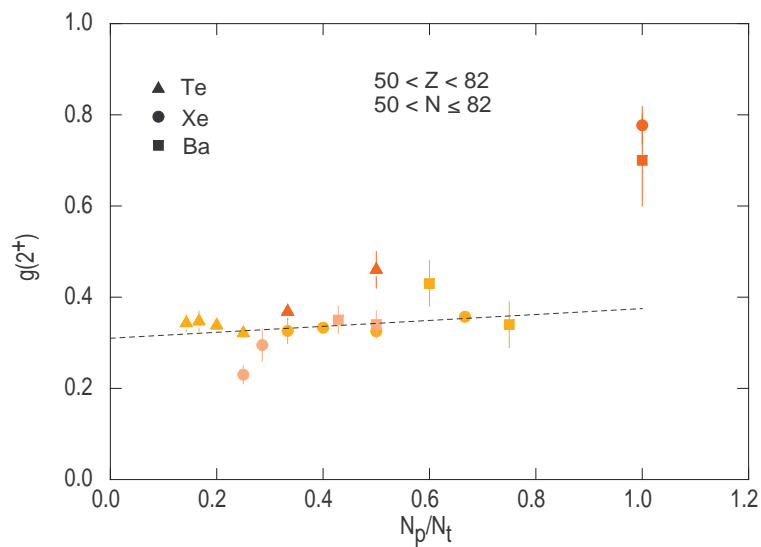


Figure 3. Similar to figure 2 but for nuclei with $50 < Z < 82$ and $50 < N \leq 82$.

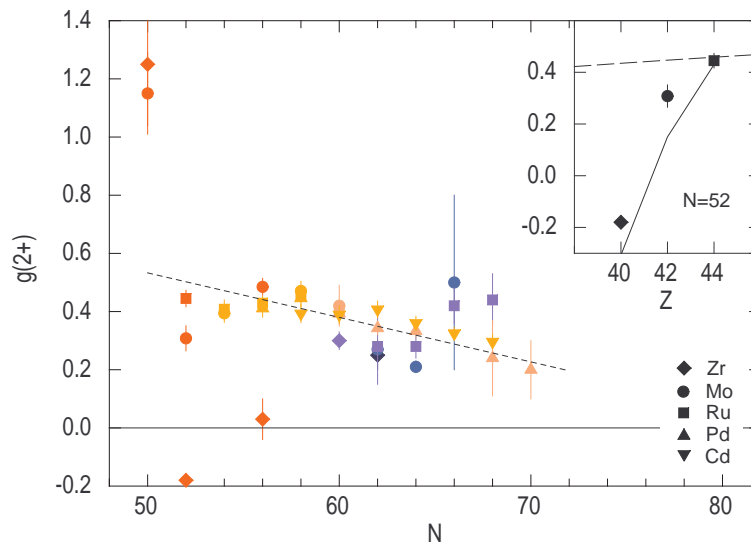


Figure 4. $g(2_1^+)$ as a function of neutron number for nuclei with $40 \leq Z < 50$ and $50 \leq N < 82$. Data are summarized in [6]. The broken line indicates the trend for $56 \leq N \leq 70$. See figure 1 for color key. The inset shows $g(2_1^+)$ for the $N = 52$ isotones. The dashed line is Z/A ; the solid line is the shell model calculation of Holt *et al.* [9].

Finally, turning to figure 4 and the $A \sim 100$ region ($40 \leq Z < 50$ and $50 \leq N < 82$), the g factors departing strongly from the trend for collective nuclides show similarities to the rare-earth region in that the proton excitations in semimagic nuclei again have $g(2_1^+) \sim 1$, and then with the addition of two neutrons, $g(2_1^+)$ falls well below the collective trend, even becoming negative in ^{92}Zr .

Whereas the behavior of $g(2_1^+)$ follows a similar path to collectivity in the $A \sim 100$ and rare earth regions, the trends differ once collectivity sets in. In the $A \sim 100$ nuclei the g factors are *not* well correlated with N_p/N_t . Instead they decrease steadily as N increases beyond mid-shell at $N = 66$. The reason for this difference will be discussed below.

3. g factors and the onset of collectivity

The phenomenon whereby $g(2_1^+)$ values drop below the collective value of $g \sim Z/A$ in nuclei with two or four neutrons outside a closed shell was noted and discussed about a decade ago [10, 11]. An important observation is that the coupling between protons and neutrons in these nuclei with few valence nucleons is rather weak. For example, the level spectrum of $^{144}_{60}\text{Nd}_{84}$ can be obtained by superimposing the level schemes of $^{142}_{60}\text{Nd}_{82}$ (the 4-proton excitation) and $^{148}_{64}\text{Gd}_{84}$ (the 2-neutron excitation; $^{148}_{64}\text{Gd}_{82}$ is approximately a closed-shell nucleus), as shown in figure 5. It was suggested that (i) coupling between the valence protons and neutrons is relatively weak because the protons and neutrons are in different shells, and (ii) neutron excitations are then favored in the lowest 2^+ state because their residual interactions are more attractive than those between protons. Considerable progress has been made since then. The shell model calculations of Holt *et al.* [9] for the $N = 52$ isotones, shown in the insert of figure 4, give a good description of the data and illuminate the underlying nuclear structure phenomena. The weak coupling of the proton and neutron excitations leads to a ‘configurational isospin polarization’, which means that the 2_1^+ and 2_2^+ states in ^{92}Zr , for example, do not form the fully-symmetric and mixed-symmetry states of the proton-neutron interacting boson model. The consequent difference in

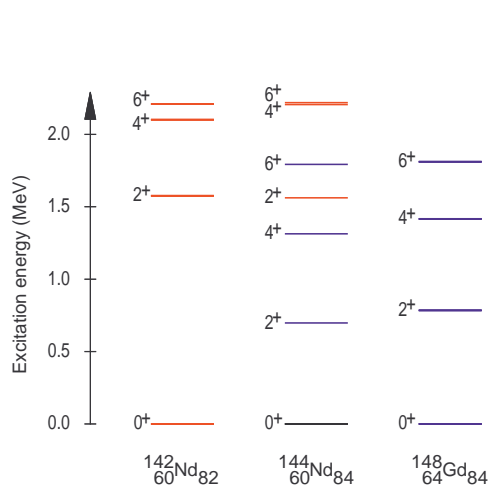


Figure 5. Level schemes demonstrating the weak coupling of proton (red) and neutron (blue) neutron excitations in ^{144}Nd .

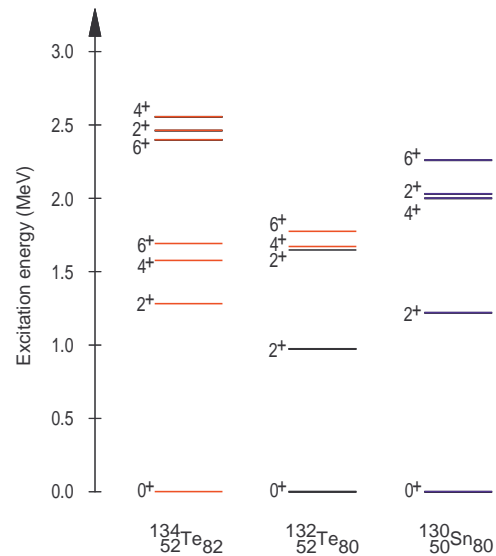


Figure 6. Similar to figure 5 but showing the similar energies of the parent proton and neutron excitations in the lowest 2^+ state of ^{132}Te .

their g factors has been observed [12].

Research into the g factors of nuclei near closed shells, the formation of mixed symmetry states, and the on-set of collectivity, is on-going. In the $A \sim 80$ region, the $N = 48$ isotones $^{84}_{36}\text{Kr}$ and $^{86}_{38}\text{Sr}$ follow the pattern of $g(2^+_1) \ll Z/A$. On the other hand nuclei in the $A \sim 130$ region do not follow the same trend. For example, $^{132}_{52}\text{Te}_{80}$, which has two valence protons and two neutron holes, has $g \sim Z/A$ [3, 4]. This case has been discussed recently by Danchev *et al.* [13]; the 2^+_1 state was populated by Coulomb excitation of a radioactive beam and identified as the first example of a mixed symmetry state in a neutron-rich nucleus.

Further insight into the different behavior of the $A \sim 130$ nuclei is gained from figure 6 wherein the level scheme of $^{132}_{52}\text{Te}_{80}$ is compared with those of $^{130}_{50}\text{Sn}_{80}$ and $^{134}_{52}\text{Te}_{82}$, which represent its constituent neutron and proton configurations, respectively. It is evident that the 2^+_1 proton excitation in ^{134}Te is nearly degenerate with the 2^+_1 neutron excitation in ^{130}Sn , and as a consequence the 2^+_1 and 2^+_2 states in ^{132}Te have about equally mixed proton and neutron components. This scenario is confirmed by shell model calculations [13]. Looking to the 4^+_1 and 6^+_1 states, it is evident from the comparison of the levels in figure 6 that, in contrast to the 2^+ states, these states in ^{132}Te are likely to be predominantly proton excitations akin to the 4^+_1 and 6^+_1 states in ^{134}Te . The measured g factors of the 6^+_1 states [8] are $g(^{134}\text{Te}) = +0.847(25)$ and $g(^{132}\text{Te}) = +0.78(8)$, giving further evidence that both states are essentially the same proton excitation.

A comparison of the level schemes of $^{130}_{52}\text{Te}_{78}$, $^{128}_{50}\text{Sn}_{78}$ and $^{134}_{52}\text{Te}_{82}$ shows that with the removal of a further two neutrons, the relative level ordering remains very like the case of ^{132}Te . It is to be expected, therefore, that in ^{130}Te the lowest two 2^+ states are mixed proton-neutron excitations, whereas the 4^+_1 state is predominantly a proton excitation. An experiment is planned at the Australian National University to measure these three g factors in ^{130}Te simultaneously by the transient-field method [14]. As more comprehensive data are obtained concerning the g factors of excited states near closed shells, it will help develop deeper insights into the formation of mixed symmetry states and the on-set of collectivity in atomic nuclei.

4. Global trends in collective g factors

As noted above, the behavior of $g(2_1^+)$ follows a similar path to collectivity in the $A \sim 100$ and rare earth regions, but the trends differ once collectivity sets in. Why the difference? It must stem from the sensitivity of the g factors to the underlying single-particle composition of the quadrupole collectivity.

The question has been illuminated by microscopic calculations using the tidal-wave model of Frauendorf and collaborators [6]. This model, which describes the yrast states of transitional and deformed nuclei by means of the self-consistent cranking model, allows the calculation of the magnetic moment directly from the nucleonic currents. It was found that the decrease in $g(2_1^+)$ along the isotope chains in the $A \sim 100$ region is primarily due to an increasing angular momentum contribution from the $h_{11/2}$ neutrons, which can begin even below $N = 64$, as illustrated for the Mo isotopes in figure 7. The mechanism is akin to the strong increase of angular momentum carried by neutrons in deformed nuclei, caused by the rotational alignment of the $i_{13/2}$ and $j_{15/2}$ neutrons, which reduces the g factors of high-spin states below Z/A .

It is therefore proposed that the difference in the g -factor systematics observed for the $N = 50 - 82$ shell compared to the $N = 82 - 126$ shell stems from the difference in the location of the high-spin intruder orbital. As seen in figure 7, the neutron $h_{11/2}$ orbit is near the top ($N = 82$ end) of the $N = 50 - 82$ shell. In contrast, the $i_{13/2}$ orbit is much nearer to the middle of the $N = 82 - 126$ shell. A study of the data in figure 2 in the tidal-wave model is needed. The aim would be to provide a microscopic basis for the trends observed, including the trend of rising g factors towards the $N = 126$ end of the shell.

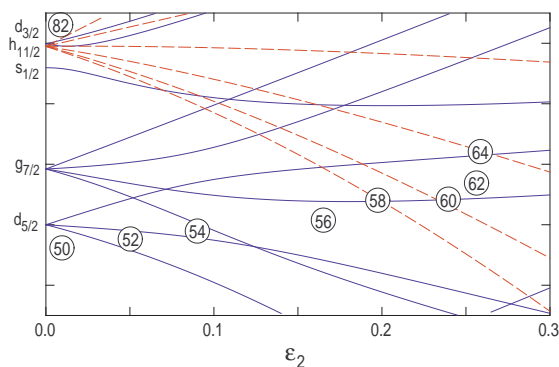


Figure 7. Nilsson diagram for neutrons in Mo isotopes, which illustrates the intrusion of the $h_{11/2}$ shell among the positive parity orbits and the consequent impact of $h_{11/2}$ orbit on the g factors in this region [6]. Neutron numbers are indicated at the calculated deformations.

5. Moment measurements on radioactive beams: the Recoil in Vacuum method

It is apparent from the preceding discussion that g -factor measurements can give useful insights into nuclear structure, both to understand global trends and the details of specific regions. However, as indicated in figure 1, $g(2_1^+)$ measurements are at present largely confined to stable nuclides. This limitation is being overcome through measurements on radioactive beams. In this section attention turns to some developments related to the recoil in vacuum method.

When a free ion moves through vacuum, the hyperfine interaction couples the atomic spin \mathbf{J} to the nuclear spin \mathbf{I} and together they precess about the total spin $\mathbf{F} = \mathbf{I} + \mathbf{J}$. The precession frequency $\omega_{F,F'}$ is proportional to the nuclear g factor and the magnitude of the hyperfine magnetic field at the nucleus. To measure the g factor, the nuclear state of interest is excited by a suitable reaction and then allowed to recoil into vacuum. The effect of the hyperfine interaction is observed via the perturbation of the angular correlation of the γ -rays de-exciting the state. The difference between the perturbed angular correlation and the unperturbed angular correlation is described by the vacuum attenuation coefficients, G_k ($k = 2, 4$), which also contain the information about the nuclear g factor. This recoil in vacuum (RIV) method has proved

suitable to measure excited-state g factors in unstable nuclei, especially neutron-rich nuclei produced as radioactive beams [3, 4]. For further details of the method and notation, see [4] and references therein.

The RIV method has a number of advantages for applications to radioactive beams, one being that both the g factor and the $B(E2; 0 \rightarrow 2)$ can be determined in the same experiment. At the Australian National University we have been studying the free-ion hyperfine fields of stable nuclei having known moments with a view to the applications of the RIV technique to radioactive beams. These free-ion fields must be characterized in order to extract the nuclear g factor from the measured attenuation coefficients, G_k . In contrast to the radioactive beam measurements, which use large arrays of particle and γ -ray detectors with large solid angle coverage, the stable beam measurements have been made with modest apparatus. Four HPGe γ -ray detectors operate in coincidence with an array of eight photodiode particle detectors called ‘Heliotrope’ placed around the beam axis at forward angles ($\sim 30^\circ$). Like the radioactive beam measurements, the stable-beam studies have been performed in inverse kinematics with the beam ions Coulomb excited on either ^{12}C or ^{27}Al targets; the different targets serve to vary the exit velocity and hence charge-states of the ions entering vacuum.

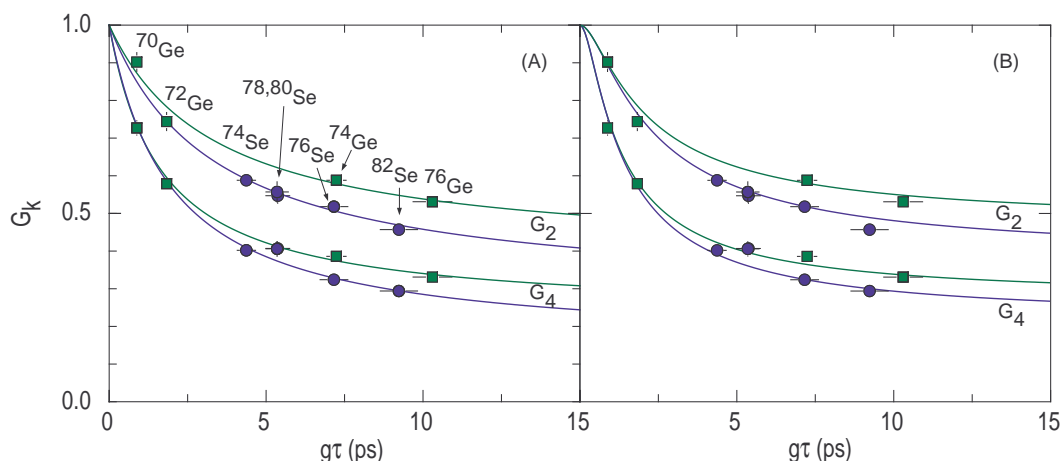


Figure 8. Vacuum deorientation coefficients for the stable isotopes of Ge and Se after excitation of 175 MeV beams on carbon targets. (A) Solid lines are empirical fits to equation 1. (B) Lines are model-based fits assuming gaussian field distributions (see text).

Figure 8 shows measured attenuation coefficients, G_k , for 175 MeV beams of the stable ^{32}Ge and ^{34}Se isotopes excited on a carbon target. As in previous work, the G_k values are plotted as a function of the product of the g factor and the mean life of the 2_1^+ states. The observed difference in the attenuation for the longer-lived isotopes, i.e. $^{74,76}\text{Ge}$ compared with $^{76,82}\text{Se}$, was surprising. The measurements were therefore repeated and subjected to extensive checking. For example, a cocktail beam of ^{74}Ge and ^{74}Se was used to perform simultaneous measurements of the vacuum attenuation for these two ions.

We do not yet have a ‘first-principles’ atomic physics explanation for this difference between the hyperfine fields for Ge and Se ions recoiling in vacuum under almost identical conditions. However some important conclusions can be drawn based on empirical and semi-empirical fits to the data. The left panel in figure 8 shows an empirical fit based on

$$G_k = \alpha_k + (1 - \alpha_k) \frac{C_k}{C_k + g\tau}, \quad (1)$$

where α_k and C_k are parameters that must be fitted separately to G_2 and G_4 . The ‘hard core’ parameter α_k gives the asymptotic value of G_k at long times, while C_k is the time constant for the quasi-exponential decay of the attenuation coefficient. Physically, C_k is related to the average strength of the hyperfine fields acting on the nucleus, while α_k is determined by the average angular momentum of the atomic electron configurations.

The right panel of figure 8 shows a semi-empirical model-based fit to the data. This static-model fit method has been described in [4]. It assumes that the vacuum attenuation results from the superposition of hyperfine fields with gaussian distributions in atomic spin and field strength. To limit the parameters it has proved effective to (i) fix the standard deviation of the atomic spin to $\sigma_J = 1\hbar$, and (ii) for the distribution of hyperfine fields, to set $\sigma_B = \bar{B}$, where \bar{B} is the average hyperfine field strength at the nucleus. Two parameters, \bar{J} and \bar{B} , then determine G_2 and G_4 .

Both the empirical fit (with 4 parameters) and the semi-empirical model-based fit (with 2 parameters) give comparable descriptions of the data. Moreover, both fits show that effectively the *same* average hyperfine field strength is experienced by the Ge and Se ions. What differs for the Ge versus Se ions is the magnitude of the hard core term in the empirical fit or, equivalently, the value of \bar{J} in the model-based fit. Specifically, $\bar{J} = 1.2$ for Ge and $\bar{J} = 1.7$ for Se.

Charge-state measurements (performed at the Australian National University) suggest that the Ge ions here carry on average 12 to 13 electrons, whereas the Se ions on average carry 15. The Ge ions are therefore mainly Mg-like and Al-like, with ground state configurations of $3s^2$ and $3s^23p^1$, respectively. These configurations produce the terms 1S and 2D , respectively, with corresponding ground-state atomic spins of $J = 0$ and $J = 1/2$. For P-like ions the lowest configuration is $3s^23p^3$, which produces the terms 4S , 2D , and 2P , and the ground-state spin is $J = 3/2$. These observations are qualitatively consistent with the experimental evidence that \bar{J} is slightly higher for Ge than for Se. Also, the low-excitation spectra of excited Mg-, Al- and P-like ions are consistent with an average atomic spin in the range $1 \leq \bar{J} \leq 2$.

Figure 9 shows how the hard core parameters depend on the atomic angular momentum J . The magnitude of the hard-core is a very strong function of J for $J < 2$, but becomes almost independent of the atomic angular momentum for $J \geq 2$. It can be concluded that the strong

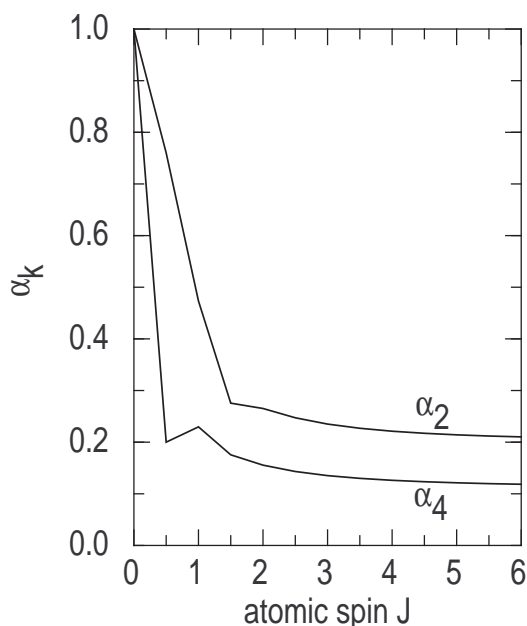


Figure 9. Atomic spin dependence of the hard-core vacuum-deorientation coefficients.

sensitivity of the hard-core attenuation observed for Se and Ge ions here is a consequence of their average atomic spin being less than $2\hbar$. In cases where $\bar{J} \geq 2$, less sensitivity to the atomic number and recoil velocity, both of which affect the average atomic configuration, is expected.

Further experiments are underway to investigate the velocity dependence of these hyperfine fields and perform detailed measurements of the relevant charge-state distributions. Calculations of the hyperfine fields for specific atomic configurations are being pursued to provide a more quantitative explanation of the free ion hyperfine fields of these highly charged ions. Due to their strong sensitivity to the average atomic angular momentum, the above data for Ge and Se ions provide a stringent test for ‘first-principles’ atomic calculations of free ion hyperfine fields (see for example, [15]).

6. Summary and Conclusion

Patterns in $g(2_1^+)$ systematics for heavy nuclei have been examined and found to be sensitive to the underlying single-particle structure. Near closed shells the magnetic moments can show pronounced changes that depend on the strength of the coupling between protons and neutrons. Beams of radioactive ions are enabling the extension of the $g(2_1^+)$ data to include unstable nuclei, especially neutron-rich isotopes.

The RIV method has proved useful for magnetic moment measurements on the first-excited states of unstable nuclei produced as radioactive beams. Experiments on stable beams with known moments are underway at the Australian National University to characterize the free ion hyperfine fields, which must be understood to fully exploit the RIV method. An unexpected difference between the hyperfine fields for Ge and Se ions recoiling in vacuum under similar conditions can be attributed to their average atomic angular momentum being between 1 and $2\hbar$. Such cases will provide a sensitive testing ground for atomic physics calculations that seek to calculate the hyperfine fields from first principles.

Acknowledgments

The author is grateful to many colleagues who have made the work discussed here possible. Russell Leslie in particular is thanked for his contributions to the measurements described in section 5. This research was supported in part by the ARC Discovery Scheme, Grant No. DP0773273.

References

- [1] Cejnar P, Jolie J and Casten R F 2010 *Rev. Mod. Phys.* **82** 2155
- [2] Cakirli R B and Casten R F 2006 *Phys. Rev. Lett.* **96** 132501
- [3] Stone N J *et al* 2005 *Phys. Rev. Lett.* **94** 192501
- [4] Stuchbery A E and Stone N J 2007 *Phys. Rev. C* **76** 034307
- [5] Berant Z *et al* 2009 *Phys. Rev. C* **80** 057303
- [6] Chamoli S K *et al* 2011 *Phys. Rev. C* **83** 054318
- [7] Stuchbery A E 1995 *Nucl. Phys. A* **589** 222
- [8] Stone N J 2011 **INDC(NDS)-0594** <http://www-nds.iaea.org/publications/indc/indc-nds-0594/>
- [9] Holt J D, Pietralla N, Holt J W, Kuo T T S and Rainovski G 2007 *Phys. Rev. C* **76** 034325
- [10] Stuchbery A E 2001 *Nuclear Physics A* **682** 470
- [11] Mantica P F, Stuchbery A E, Groh D E, Prisciandaro J I and Robinson M P 2001 *Phys. Rev. C* **63** 034312
- [12] Werner V *et al* 2008 *Phys. Rev. C* **78** 031301
- [13] Danchev M *et al* 2011 *Phys. Rev. C* **84** 061306
- [14] Stuchbery A E *et al* 2007 *Phys. Rev. C* **76** 034306
- [15] Stone N J, Stone J and Jonsson P 2010 *Hyperfine Interactions* **197** 29